Impact of polarized nanotube surface on ultrathin mesogen film properties: Computer simulation study

Krzysztof Górny,* Violetta Raczyńska, Przemysław Raczyński, and Zbigniew Dendzik
Institute of Physics, University of Silesia, Chorzów, Poland
and Silesian Centre of Education and Interdisciplinary Research, 75 Pułku Piechoty 1a, 41-500 Chorzów, Poland

Szymon Starzonek
Institute of High Pressure Physics, Polish Academy of Sciences, Sokołowska 29/37, 01-142 Warsaw, Poland

(Received 12 September 2018; published 7 February 2019)

We studied properties of monolayer films of *n*-cyanobiphenyl (with $n = 5, \ldots, 8$) series of mesogens anchored on the surface of single walled boron nitride nanotube. In order to assess the impact of substrate polarization on the ordering effects we compare translational and reorientational dynamics of the films with the characteristics of analogous carbon and silicon carbide nanotube based systems. We observed significant increase of the ordering degree accompanied by increased thermal stability. This ordering is less selective than those induced by the silicon carbide nanotube, which were previously reported. The antiparallel orientation of the nearest neighboring mesogens is predominant, while the system does not exhibit any long-range spatial correlations which indicates that the size of the domains is constrained to this region. These features might be of potential importance in the design of novel optoelectronic devices.

DOI: 10.1103/PhysRevE.99.022701

I. INTRODUCTION

Molecular systems encapsulated in carbon nanotubes or physisorbed on their surface have been studied for both fundamental scientific reasons as well as for potential practical applications [1–3]. Many experimental efforts have also been devoted to study the properties of liquid crystals with dispersed carbon nanotubes [4–9].

Properties of thin mesogen films anchored on a variety of substrates have gained considerable attention due to their extraordinary features which make them novel materials for optoelectronics [10–12] as well as promising bases for biochemical sensing devices [13]. Moreover, they have strong influence on new approaches for theoretical description of liquid crystals physics. Optical properties of thin molecular layers (e.g., transparency) as well as the ability to switch between orientational configurations easily and in a controlled manner makes them good materials for display devices and transoptors. Significant development in the field of computational techniques, stimulated by the progress in accessible hardware, has enabled precise modeling of such systems [14,15]. Computer simulations have been used to study the wetting of a crystalline substrate by nematic nanodroplets [11] and the anchoring of mesogens on the surface of organic self-assembled monolayers [12]. In particular, it was shown that the quality of these self-assembled substrates considerably affects the ordering of the mesogen layer. It was also demonstrated that the interface between the thin layer and "vacuum" has also a significant impact on this ordering, what may suggest strong impact of negative pressures and needs to be described using critical-like behavior. However, such an approach will not be discussed in this paper.

The proper ordering and alignment of liquid crystals is a key feature that determines the practical feasibility of a mesogen based device. Increasing the ordering of the system is one of the fundamental goals of liquid crystal research. Understanding the origin of such a mechanism on the molecular level is still insufficient. Liquid crystals are especially sensitive to the processes taking place at interfaces [12].

Orientational ordering, electric, and dielectric properties of liquid crystals can be strongly affected by anchoring them on different substrates such as graphene [16] or carbon nanotubes [17]. The ordering of *n*-cyanobiphenyl (nCB) mesogen films adsorbed on the surface of carbon nanotubes has been shown to exhibit odd-even effects, similar to the films adsorbed on the surface of SiC nanotubes, while the latter system shows a more selective diffusion pattern [15]. In this work, we extend our previous studies on the effect of anchoring on properties of ultrathin nCB layers and impact of nanotubes surface polarization by studying the dynamics of nCB thin films physisorbed on a boron nitride nanotube outer surface.

II. SIMULATION DETAILS

We have performed a series of MD simulations using NAMD 2.11 [18] code. Visualizations were performed using VMD software [19]. Boron-nitride armchair nanotube (BNNT) was treated as rigid body and its interactions with environment was modeled as described by Won and Aluru [20]. Polarization of BNNT surface was taken into account and partial charges were set to be equal to $0.4e$ for B atoms and -0.4 for N atoms, to reflect the polarization of the nanotube in a nonpolar environment [20]. The BNNT chirality

*krzysztof.gorny@us.edu.pl

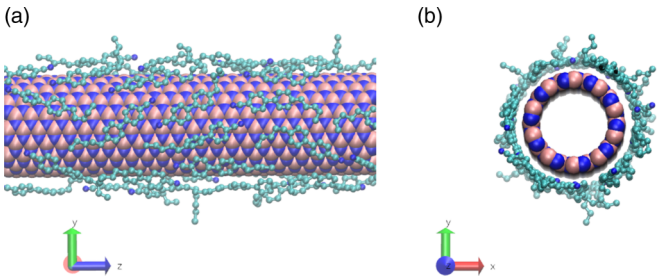

FIG. 1. 5CB mesogen film on the surface of boron nitride nanotube at $T = 350$ K—snapshot of the instantaneous configuration.

(10, 10) was chosen to have similar diameter (approximately 1.3 nm) as the carbon nanotube in our previous study [15]. The nCB mesogen molecules were described using a model developed by Tiberio and co-workers [14]. Nonbonded interactions were cut off at the distance of 2 nm. Long range electrostatic interactions were modeled using the particle mesh Evald summation method [21]. The equation of motions were integrated using the Brunger-Brooks-Karplus algorithm [22] implemented in NAMD. Simulation time step was set to 1 fs for all simulations presented in this study.

The model of the hexagonal boron-nitride was utilized to study transport of water in nanochannels [20], solvation of hexagonal boron-nitride in polar and nonpolar solvents [23], insertion of BNNTs into phospolipid bilayer [24], or extraction of phospholipids from bilayer [25]. The nCB mesogen model, which was optimized to correctly predict the nematic-isotropic phase transition in bulk samples, was successfully adopted to study the complex interaction between the self-assembled monolayer and nCB film [12].

Initial configurations of the simulated system were obtained from NPT simulations of BNNT immersed in bulk nCB matrix. Excess nCB molecules were removed from the system until a one-molecule thick layer of nematic molecules surrounding the nanotube remained. After each exclusion, auxiliary NVT simulations were performed to test whether the nCB molecules form a uniform, one-molecule thick layer. Initial configurations were composed of BNNT, aligned along Z axis, with 40 5CB or 38 6CB or 36 7CB or 34 8CB molecules. Simulation cell was set to $10.0 \times 10.0 \times 6.01$ nm. Z dimension of simulation box was set to fully accommodate the BNNT. The systems were simulated in five temperatures: 270, 290, 310, 330, and 350 K. Before production runs the systems were equilibrated for 5 ns for each temperature. The production runs were 20 ns long. For each nCB family member and each temperature the production runs were repeated 45 times and the results were averaged over all trajectories. Figure 1 shows a snapshot of the simulated system retrieved from randomly chosen trajectory.

III. RESULTS AND DISCUSSION

In order to assess the uniformity of the layers, we calculated density profiles of thin films of different nCB series. Figure 2 shows the mean values of density calculated for different lengths of the mesogen. The insets show density profiles calculated for Z and R axes of the cylindrical frame

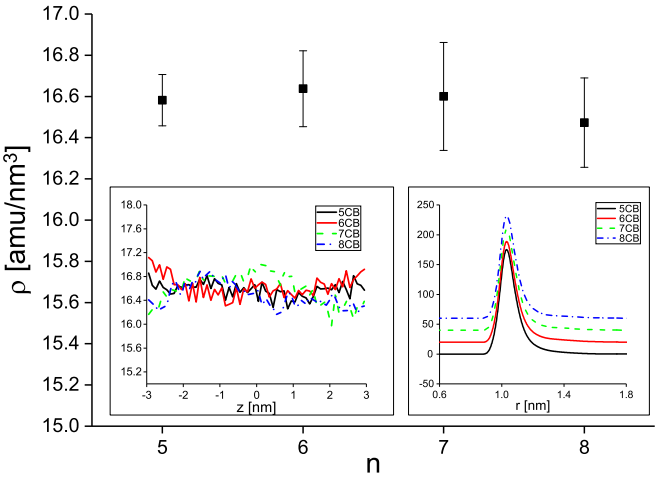

FIG. 2. Mean value of the nCB mesogen layer density profile along the z axis obtained for a single simulation run at $T = 310$ K. The insets show the density profiles of the layer along the z axis (left inset) and along the r axis of the cylindrical frame aligned with nanotube (right inset; each curve has been shifted by 20 units to improve clarity).

associated with the nanotube (calculated from a randomly chosen trajectory). Density profiles were calculated using Density Profile Tool for VMD [26]. All density profiles along the Z axis (corresponding to the main axis of the nanotube) exhibit no significant discontinuities. Only very limited local density fluctuations occur. The profiles along the R axis are almost identical for the films composed of different mesogens, which indicates similar thickness and density of the layers.

Orientational order of the ensemble can be characterized by the order parameter $\langle P_2 \rangle$, describing ordering of the liquid crystal molecules with respect to director $\mathbf{n}$. The values of $\langle P_2 \rangle$ and $\mathbf{n}$ can be calculated from the largest eigenvalue and corresponding eigenvector of the ordering matrix $\mathbf{Q}$ defined as [11]

$$\mathbf{Q} = \left\langle \frac{\sum_{i=1}^{N} [3\hat{\mathbf{u}}_i(t) \otimes \hat{\mathbf{u}}_i(t) - \mathbf{I}]}{2N} \right\rangle, \tag{1}$$

where $\hat{\mathbf{u}}(t)$ is a unit vector along the selected molecular axis, $\mathbf{I}$ is the 3×3 identity matrix, $\mathbf{N}$ is the total number of mesogen molecules, and the time averaging is performed over all available time steps in the trajectory. The principal axis of inertia has been selected for $\hat{\mathbf{u}}(t)$.

Figure 3 shows second rank order parameter vs temperature, calculated for all mesogen films. The values of $\langle P_2 \rangle$ are considerably higher for BNNT nanotube than in the case of CNT or SiCNT [15], as well as in the case of model predictions for bulk samples [14]. Relatively high values of $\langle P_2 \rangle$ over the entire studied temperature range indicates nematic ordering of the films.

Our previous study shows the odd-even effect for the system adsorbed on SiCNT as well as CNT, while in the case of SiCNT it is considerably more pronounced than in the case of the homogenous CNT [15]. nCB films adsorbed on heterogenous BNNT exhibit an analogous odd-even pattern, although its amplitude is much smaller than for the case of

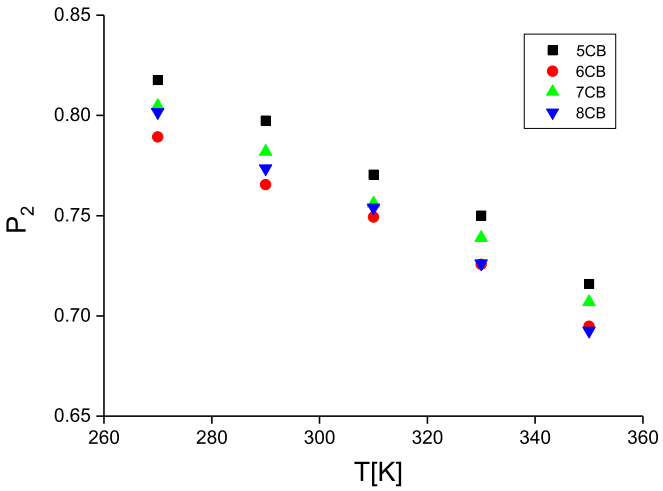

FIG. 3. Order parameter P_2 of 5CB (■), 6CB (●), 7CB (▲), and 8CB (▼) molecules on the surface of boron nitride nanotube, plotted versus temperature.

SiCNT and similar as in the case of the homogenous CNT based system. Figure 4 shows the dependence of $\langle P_2 \rangle$ on the length of the nCB hydrocarbon chain for BNNT based system compared to its CNT and SiCNT analogs [15]. The BNNT based films exhibit even higher degree of ordering than SiCNT

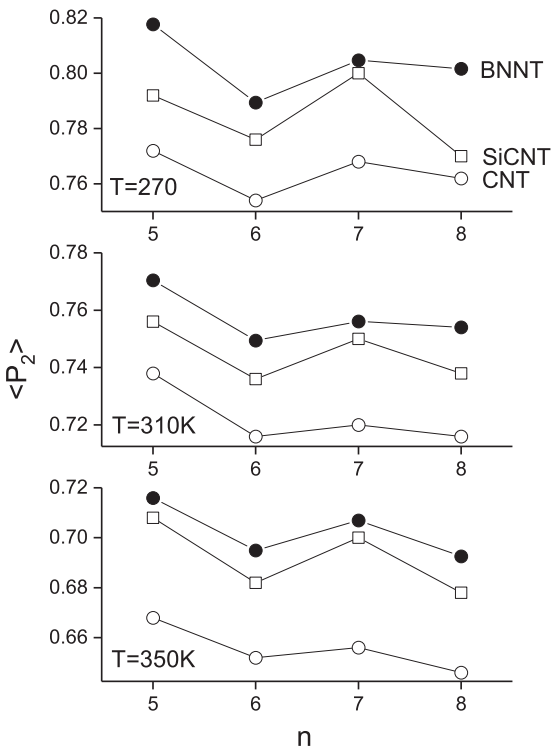

FIG. 4. Values of P_2 order parameter for 5CB, 6Cb, 7CB, and 8CB films on the surface of carbon nanotube (open circles), silicon carbide nanotube (open squares), and boron nitride nanotube (solid circles), plotted versus the number of carbon atoms (n) in the aliphatic tail of the nCB molecule, at the temperatures $T = 270$ K, $T = 310$ K, and $T = 350$ K. Data for CNT and SiCNT based films were taken from [15].

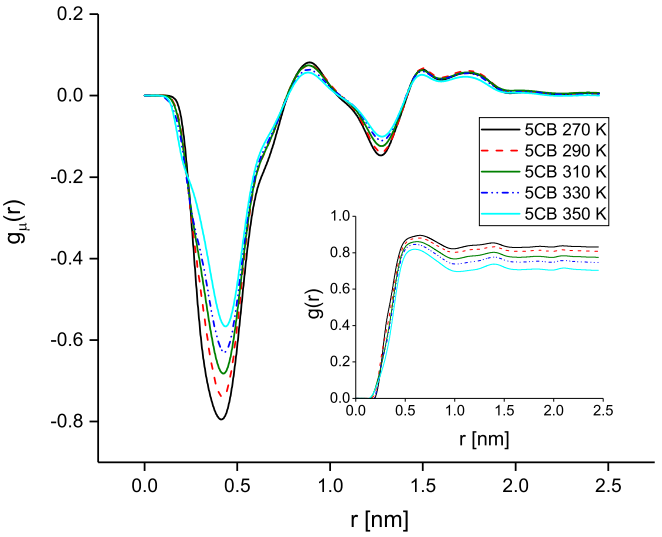

FIG. 5. Spatial correlations of 5CB thin film on the surface of boron nitride nanotube vs temperature.

based films, while preserving similar selectivity as in the case of CNT.

For nCB family members the molecule long axis and dipole moment are strongly associated with the triple carbon-nitrogen bond. This bond can be used to determine orientation of the molecule. Local organization of the sample, which is strongly reflected in the global ordering, can be measured in terms of spatial correlation defined as

$$g_\mu(r) = \frac{\sum_{i\neq j} \hat{\mathbf{u}}_i(\hat{\mathbf{r}}_i) \cdot \hat{\mathbf{u}}_j(\hat{\mathbf{r}}_j)\delta(r_{ij} - r)}{\sum_{i\neq j} \delta(r_{ij} - r)}, \tag{2}$$

where $\hat{\mathbf{u}}_\mathbf{i}(\hat{r}_i)$ is the unit vector along dipole moment μ of ith nCB molecule located at position $\hat{\mathbf{r}}_\mathbf{i}$ and $\mathbf{r}_{ij}$ is the distance between ith and jth molecule, and radial distribution function defined as

$$g(r) = \frac{1}{4\pi r^2 dr\, N} \sum_{i\neq j} \delta(r_{ij} - r), \tag{3}$$

where $\mathbf{N}$ is the number of molecules in the system and dr is radial pair distribution's bin size.

Temperature dependency of the spatial correlation function is shown in Fig. 5. The inset shows the corresponding radial distribution functions. It can be seen that the nearest neighbors retain antiparallel orientation. The increase of temperature weakens the orientational anticorrelation. Only the first coordination zone displays strong alignment of the molecules, which suggests that the correlation radius is limited to not more than 0.6 nm. The fluctuations in the long range regime do not indicate any significant repeating orientational pattern. This suggests lack of the domains larger that those composed of the nearest neighbors. This feature is also present for other nCB homologs. Figure 6 shows dependency of spatial correlations on the number of carbon atoms in the aliphatic tail of the mesogen. Position of the first minimum is shifted towards shorter distances with increasing length of the molecule. This process is reflected in radial distribution, where splitting in the short distance regime occurs. The depth of the first minimum

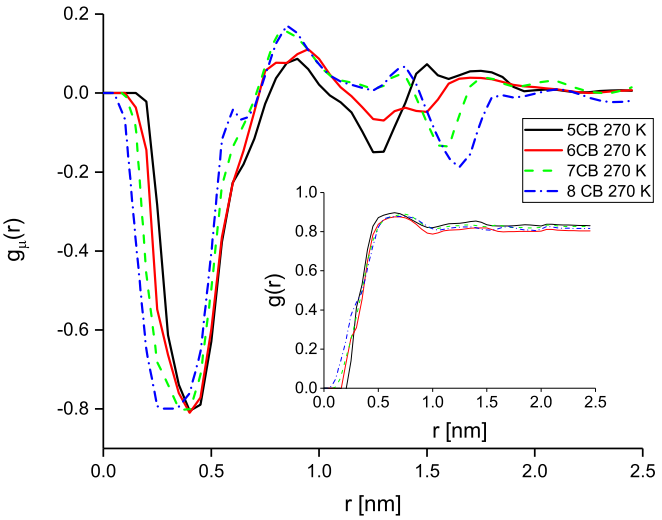

FIG. 6. Spatial correlations of nCB at the temperature $T = 270$ K.

practically does not change with the length of the mesogen, which suggests the same type of local orientational order for different members of the nCB series.

To gain deeper insight into local ordering of the systems we have calculated histograms of distribution of $\cos^2\alpha$, where α is the angle between a single molecule dipole moment and the director of the sample. The director of the sample is almost perfectly parallel to the nanotube main axis, and the laboratory frame z axis, over the entire trajectory—similar to the way reported for CNT and SiCNT based nCB films [15]. Figure 7 shows the complete set of histograms for the mesogen films based on BNNT, compared with the characteristics for the CNT and SiCNT based systems recalculated from our previous results [15]. In all cases, the mesogens of nCB films based on BNNT exhibit stronger orientational alignment compared to CNT and SiCNT based films, which corresponds to larger values of order parameter P_2. On the other hand, the BNNT based films possess a considerable amount of the molecules with orientation which significantly differs from the parallel one (between 10% and 15% of molecules with angles higher than 45°)—opposite to the CNT and SiCNT based films (for angles higher than 45° histograms vanished almost to zero). These two competitive trends are crucial to understanding the dynamics of these systems.

Translational dynamics can be assessed in terms of mean square displacement (MSD), defined as

$$\langle \Delta r^2(t) \rangle = \langle [\hat{\mathbf{r}}(t) - \hat{\mathbf{r}}(0)]^2 \rangle = 6Dt, \tag{4}$$

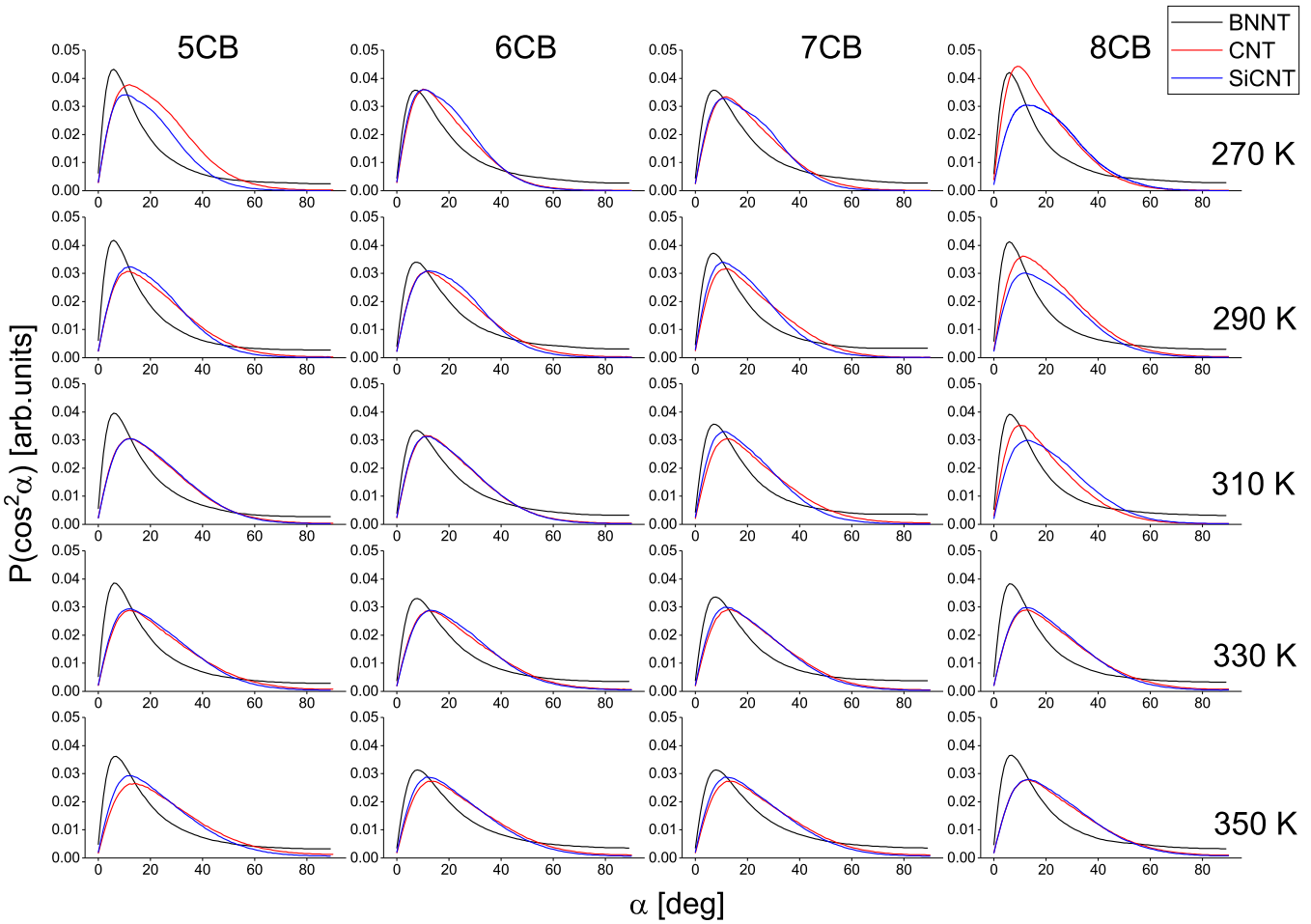

FIG. 7. Histograms of the angle of the single molecule dipole moment and global director of the sample. Data for CNT and SiCNT based films were recalculated from results published in [15].

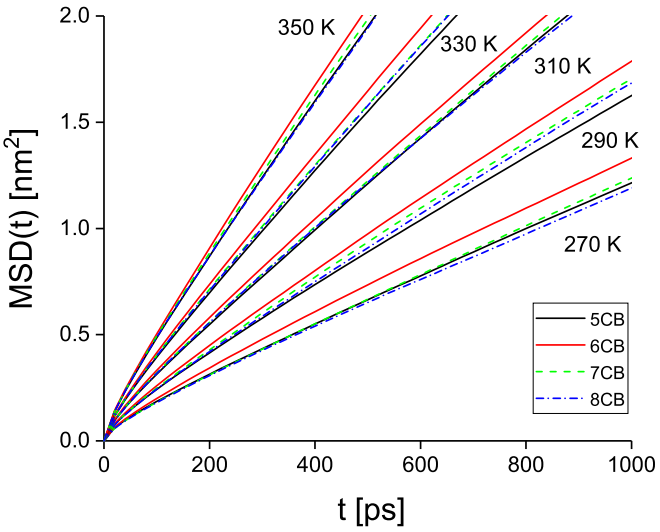

FIG. 8. Mean square displacement of nCB mesogens on the surface of boron nitride nanotube at temperatures ranging between $T = 270$ K and $T = 350$ K.

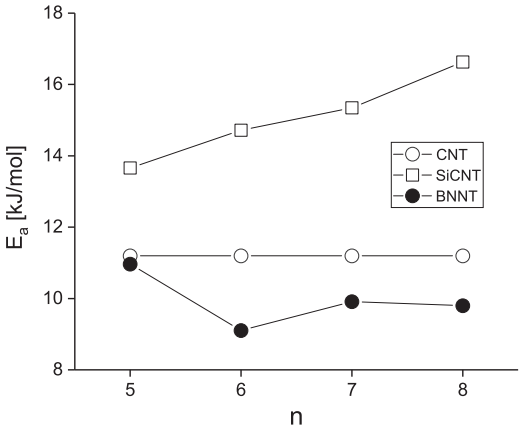

FIG. 9. Thermal activation characteristic of diffusion coefficient of nCB molecules on the surface of carbon nanotube (open symbols) [15], silicon carbide nanotube (open symbols) [15], and boron nitride nanotube (solid symbols), plotted versus the number of carbon atoms (n) in the aliphatic tail of the nCB molecule.

where **0** indicates the reference trajectory frame, $\langle\,\rangle$ denotes the average over all molecules and all available trajectory frames, and **D** is the diffusion coefficient (Einstein relation). The value of the diffusion coefficient can be influenced by the introduction of periodic boundary conditions. This effect can be mitigated by introduction of appropriate corrections [27]. This correction however concerns the case of a single molecule on the boundary between two media or in well defined continuous media. In the case of a mesogen film located on fixed substrate introduction of such correction is not applicable, as the distortion in velocity field introduced by an immobile nanotube is significant, relatively higher than the artificial effect introduced by periodic boundary conditions, and the viscosity in the interface between nematic film and vapor cannot be correctly estimated. Figure 8 presents the averaged MSD of all studied systems. In all cases, after the initial ballistic region, a well defined, linear diffusion regime can be observed. It is worth noting that the most disordered 6CB films exhibit the highest diffusion. Thermal characteristic of the translational diffusion coefficient follows very well the Arrhenius law. The values of diffusion activation energies $\mathbf{E_a}$ are shown in Fig. 9. Activation energies for BNNT based films are lower than in the case of their CNT and SiCNT counterparts and follow an interesting pattern. For 5CB diffusion activation energy is practically identical as in the case of an analogous CNT based system. What is quite unexpected is that the activation energy is the lowest in the case of the 6CB, and then increases for the next homologs, although the values for 7CB and 8CB remain considerably lower than in the case of CNT based films. Dynamical behavior is consistent with the odd-even ordering pattern of the films (Fig. 4). This can be rationalized taking into account the difference in the distribution of mesogen molecules orientation (Fig. 7). The broader spectrum of the available orientations allows more sophisticated diffusion patterns than in the case of films on SiCNT or CNT, where available orientations are much more limited. Dipolar relaxation, which can be measured with dielectric relaxation spectroscopy, is sensitive to intermolecular interactions and is able to provide information on cooperative processes, providing the link between techniques which probe the properties of individual molecules and techniques characterizing the bulk properties of the sample [2,28,29]. The characteristic of the dipolar relaxation process of a confined molecular system is an outcome of a counterbalance between two competing processes—interaction between host and guest systems and the change of the length scale of the cooperatively rearranging regions imposed by the geometrical constraints. The reorientational dynamics of the molecules is reflected in the autocorrelation of the total dipole moment of the sample,

$$\Phi(t) = \frac{\langle \mathbf{M}(0)\mathbf{M}(t)\rangle}{\langle \mathbf{M}(0)\mathbf{M}(0)\rangle}, \tag{5}$$

where **M** is the total dipole moment of the system, defined as a sum of dipole moments μ_i of mesogens. Using the procedure described in our previous papers [2,15] we recalculated the dipole moment of each mesogen for each trajectory frame, with respect to charge distribution and position of atoms in the molecule, and then summed them to obtain the total dipole moment of the mesogen film. Total dipole moment autocorrelation was then plotted $-\ln(-\ln[\Phi(t)])$ against $\ln(t)$ and fitted with the Kohlrausch-Williams-Watts (KWW) decay function

$$\Phi(t) = e^{-(t/\tau_{KWW})^{\beta}}, \tag{6}$$

where τ_{KWW} is a measure of the characteristic relaxation time and $0 < \beta < 1$ is interpreted as a measure of distribution of the relaxation time or cooperativity of the relaxation process. The mean relaxation time τ has been calculated using the following relation:

$$\tau = \int_0^{\infty} \Phi(t)dt = \frac{\tau_{KWW}}{\beta}\Gamma\left(\frac{1}{\beta}\right), \tag{7}$$

where Γ denotes the gamma Euler function. The calculated values of the mean relaxation time were then plotted on the activation plot $\ln(\tau)$ against $1/T$. Figure 10 shows dipolar relaxation thermal activation energies E_a' determined from the

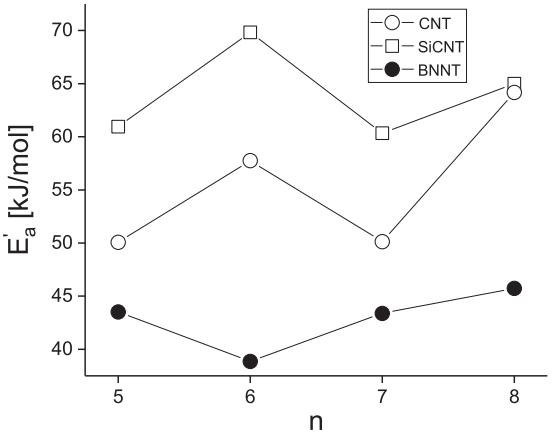

FIG. 10. Thermal activation of dipolar relaxation plotted versus the number of carbon atoms (n) in the aliphatic tail of the nCB molecule. Open symbols represent data for nCB thin films on carbon nanotube and silicon carbide nanotube [15]; solid symbols represent data for boron-nitride nanotube.

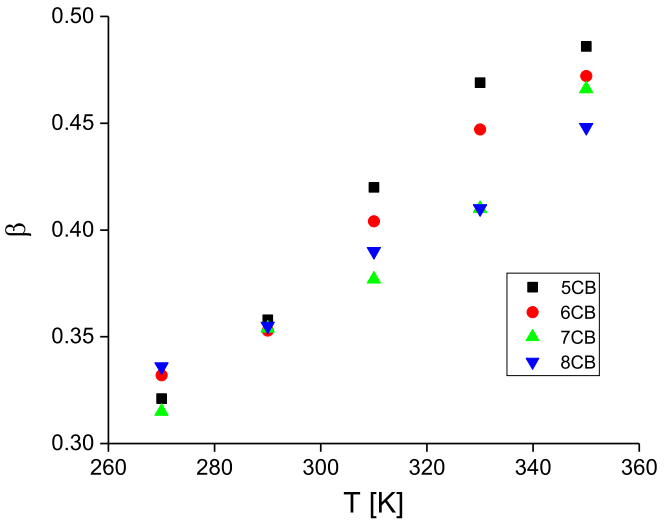

FIG. 11. Temperature dependency of the KWW parameter β of 5CB (■), 6CB (●), 7CB (▲), and 8CB (▼) molecules on the surface of carbon nanotube (open symbols), silicon carbide nanotube (solid symbols), and boron nitride nanotube (half-open symbols).

activation plot for simulated mesogen films. Activation energies for BNNT based mesogen films for all nCB homologs are lower than 46 kJ/mol, which is significantly lower than in the case of either CNT or SiCNT based systems. The activation energy of the 5CB film based on BNNT is relatively high, which is connected with a lack of orientational disorder. Again, the 6CB film exhibits the lowest activation energy which can be attributed to the fact that the 6CB homolog is the first one which exhibits considerable contribution of orientational disorder. In the higher nCB homologs, 7CB and 8CB, the orientational disorder is mitigated by the odd-even effect connected to increasing length of the molecule. In the case of CNT as well as SiCNT based films, which do not exhibit any considerable amount of mesogens which are not aligned along the nanotube main axis, the odd-even effect is predominant.

Figure 11 shows temperature dependence of the KWW parameter β. As one would expect, the values of β increase with temperature, which corresponds to the transition from a more collective relaxation to a single molecule process. For the temperatures higher than $T = 310$ K, this process is affected by the length of the molecule—the shorter molecules exhibit smaller deviation from an exponential (Debye) relaxation characteristic.

The nCB mesogen model developed by Tiberio *et al.* well reproduces the value of the pseudocritical exponent of the Haller equation [14] in accordance with experimental results of [30]. Our model of interactions between nanotube and mesogen correctly reproduces the theoretical prediction of uniaxial ordering of mesogen on a nanotube surface [31], as well as the Arrhenius characteristic of thermal activation of the dielectric relaxation for 5CB molecules [32]. The predominant antiparallel orientation of molecules on a polarized nanotube surface is similar to the pretransitional effect reported for 5OCB doped with ferrolectric nanoparticles [33].

The reported odd-even effect cannot be directly related only to the decrease of the configurational entrophy as suggested in [34]. If this was the case, we would observe the monotonic behavior of the order parameter with the increase of the alkyl chain length rather than an odd-even pattern. In our case, the emergence of the odd-even effect is more likely to arise from the dipole-dipole interactions related with the change in the alkyl chain. The decrease of the odd-even effect amplitude related with the introduction of the polarized BNNT surface, comparing with the CNNT case, suggests rather that this effect is the outcome of the counterbalance between dipole-dipole interactions and the reduction of the configurational entropy associated with longer hydrocarbon chains. Additionally, spatial correlations presented in Fig. 6 show that the increase of the length of the nCB molecule is accompanied by closer antiparallel pairing of the mesogen's dipoles, indicating that the odd-even effect is driven by the dipole-dipole interactions and the hydrocarbon chain length effect simultaneously.

IV. CONCLUSIONS

The obtained results suggest that the introduction of substrate polarization, which is the case of BNNT, leads to substantial changes in molecular organization and dynamics of thin mesogen films. The angle distribution of molecules on the surface of BNNT differs considerably from the systems anchored on a nonpolar surface of CNT with practically identical surface morphology and diameter. Substrate polarization enhances the global ordering of the film, but also introduces some local distortions in the film structure. These distortions lead to considerably altered dynamics, which interferes with the odd-even patterns observed in this kind of system. Polarized surface of BNNT induces an increase of the order parameter for all nCB homologs in comparison to thin films on carbon or silicon-carbide nanotubes. The magnitude of the odd-even effects is similar to that in the case of carbon nanotube based films. Apart from the changes in degree of ordering, significant decrease of the activation energies of translational as well as rotational dynamics is observed.

Replacing nonpolar CNT with its polar boron-nitride counterpart results in a considerably increased degree of nematic order accompanied with the decrease of dielectric strength being the result of the predominant antiparallel orientation of mesogens. The presented results suggest that the mesogens doped with ferroelectric nanoparticles may be of particular interest as regards potential applications in optoelectronics, because of enforcing the mutual orientation of molecules, increase in ordering, and reduction of reorientational activation energy.

ACKNOWLEDGMENTS

This research was supported in part by PAAD Infrastructure co-financed by Operational Programme Innovative Economy, Objective 2.3.

[1] M. Rahman and W. Lee, J. Phys. D: Appl. Phys. **42**, 063001, 1 (2009).
[2] Z. Dendzik, K. Górny, and Z. Gburski, J. Phys.: Condens. Matter **21**, 425101, 1 (2009).
[3] C. Chiccoli, P. Pasini, L. R. Evangelista, R. T. D. Souza, and C. Zannoni, Mol. Cryst. Liq. Cryst. **576**, 42 (2013).
[4] S. Schymura, M. Kühnast, V. Lutz, S. Jagiella, U. Dettlaff-Weglikowska, S. Roth, F. Giesselmann, C. Tschierske, G. Scalia, and J. Lagerwall, Adv. Funct. Mater. **20**, 3350 (2010).
[5] M. S. E. Peterson, G. Georgiev, T. J. Atherton, and P. Cebe, Liq. Cryst. **45**, 450 (2018).
[6] L. N. Lisetski, S. S. Minenko, A. P. Fedoryako, and N. I. Lebovka, Physica E **41**, 431 (2009).
[7] L. N. Lisetski, S. S. Minenko, V. V. Ponevchinsky, M. S. Soskin, A. I. Goncharuk, and N. I. Lebovka, Materialwiss. Werks. **42**, 5 (2011).
[8] L. N. Lisetski, S. S. Minenko, A. N. Samoilov, and N. I. Lebovka, J. Mol. Liq. **235**, 90 (2017).
[9] A. N. Samoilov, S. S. Minenko, L. N. Lisetski, E. A. Solovyova, N. I. Lebovka, and M. V. Vistak, Funct. Mater. **24**, 383 (2017).
[10] W. Gwizdala, K. Gorny, and Z. Gburski, Spectrochim. Acta A **79**, 701 (2011).
[11] O. M. Roscioni, L. Muccioli, R. G. Della Valle, A. Pizzirusso, M. Ricci, and C. Zannoni, Langmuir **29**, 8950 (2013).
[12] O. M. Roscioni, L. Muccioli, and C. Zannoni, ACS Appl. Mater. Inter. **9**, 11993 (2017).
[13] J. A. Moreno-Razo, E. J. Sambriski, N. L. Abbott, J. P. Hernandez-Ortiz, and J. J. de Pablo, Nature (London) **485**, 86 (2012).
[14] G. Tiberio, L. Muccioli, R. Berardi, and C. Zannoni, Chem. Phys. Chem. **10**, 125 (2009).
[15] K. Gorny, P. Raczynski, Z. Dendzik, and Z. Gburski, J. Phys. Chem. C **119**, 19266 (2015).
[16] T. M. Alam and C. J. Pearce, Chem. Phys. Lett. **592**, 7 (2014).
[17] V. Manjuladevi, R. K. Gupta, and S. Kumar, J. Mol. Liq. **171**, 60 (2012).
[18] J. C. Phillips, R. Braun, W. Wang, J. Gumbart, E. Tajkhorshid, E. Villa, C. Chipot, R. D. Skeel, L. Kalé, and K. Schulten, J. Comput. Chem. **26**, 1781 (2005).
[19] W. Humphrey, A. Dalke, and K. Schulten, J. Mol. Graphics **14**, 33 (1996).
[20] C. Y. Won and N. R. Aluru, J. Phys. Chem. C **112**, 1812 (2008).
[21] T. Darden, D. York, and L. Pedersen, J. Chem. Phys. **98**, 10089 (1993).
[22] A. Brunger, C. L. Brooks, and M. Karplus, Chem. Phys. Lett. **105**, 495 (1984).
[23] T. K. Mukhopadhyay and A. Datta, J. Phys. Chem. C **121**, 811 (2017).
[24] M. Thomas, M. Enciso, and T. A. Hilder, J. Phys. Chem. B **119**, 4929 (2015).
[25] Z. Li, Y. Zhang, C. Chan, C. Zhi, X. Cheng, and J. Fan, ACS Nano **12**, 2764 (2018).
[26] T. Giorgino, Comput. Phys. Commun. **185**, 317 (2014).
[27] P. Popov, L. Steinkerchner, and E. K. Mann, Phys. Rev. E **91**, 053308 (2015).
[28] M. Paluch, Z. Dendzik, and S. J. Rzoska, Phys. Rev. B **60**, 2979 (1999).
[29] U. Schneider, R. Brand, P. Lunkenheimer, and A. Loidl, Eur. Phys. J. E **2**, 67 (2000).
[30] I. Chirtoc, M. Chirtoc, C. Glorieux, and J. Thoen, Liq. Cryst. **31**, 229 (2004).
[31] N. R. Jber, A. A. Rashad, and M. S. Shihab, J. Mol. Struct. **1043**, 28 (2013).
[32] A. Drozd-Rzoska, S. J. Rzoska, and K. Czupryñski, Phys. Rev. E **61**, 5355 (2000).
[33] S. Starzonek, S. J. Rzoska, A. Drozd-Rzoska, K. Czupryński, and S. Kralj, Phys. Rev. E **96**, 022705 (2017).
[34] P. Popov, D. J. Lacks, A. Jákli, and E. K. Mann, J. Chem. Phys. **141**, 054901 (2014).